

## Engineering Conferences International ECI Digital Archives

---

10th International Conference on Circulating  
Fluidized Beds and Fluidization Technology -  
CFB-10

Refereed Proceedings

---

Spring 5-3-2011

# Characteristics of the Solid Volume Fraction Fluctuations in a CFB

Sirpa Kallio

*VTT Technical Research Centre of Finland, Finland*

Juho Peltola

*VTT Technical Research Centre of Finland, Finland*

Veikko Taivassalo

*VTT, Finland*

Follow this and additional works at: <http://dc.engconfintl.org/cfb10>



Part of the [Chemical Engineering Commons](#)

---

### Recommended Citation

Sirpa Kallio, Juho Peltola, and Veikko Taivassalo, "Characteristics of the Solid Volume Fraction Fluctuations in a CFB" in "10th International Conference on Circulating Fluidized Beds and Fluidization Technology - CFB-10", T. Knowlton, PSRI Eds, ECI Symposium Series, (2013). <http://dc.engconfintl.org/cfb10/63>

This Conference Proceeding is brought to you for free and open access by the Refereed Proceedings at ECI Digital Archives. It has been accepted for inclusion in 10th International Conference on Circulating Fluidized Beds and Fluidization Technology - CFB-10 by an authorized administrator of ECI Digital Archives. For more information, please contact [franco@bepress.com](mailto:franco@bepress.com).

# CHARACTERISTICS OF THE SOLID VOLUME FRACTION FLUCTUATIONS IN A CFB

Sirpa Kallio, Juho Peltola, Veikko Taivassalo  
VTT Technical Research Centre of Finland  
P.O.Box 1000, FI-02044 VTT, Finland

## ABSTRACT

In the paper, the fluctuation characteristics of the solids volume fraction in a CFB are evaluated from measurements and Eulerian-Eulerian CFD simulations. In both cases, similarly large fluctuations are observed in the intermediate voidage range whereas dense and dilute suspension regions are more uniform, as expected. The frequency distributions of solids volume fraction are classified to represent three different suspension density regimes: dilute, dense and intermediate "bimodal" regimes.

## INTRODUCTION

Gas-solid flow in a CFB is governed by strong fluctuations in the local solid volume fraction  $\alpha_s$ . In addition to the hydrodynamics of a CFB process, heat transfer, the distribution of reagents and the chemical reactions are also strongly affected by the distribution of  $\alpha_s$ . Hence accurate information on the solids distribution is vital for modelling any CFB process.

Bai & al. (1) and Issangaya et al. (2) analysed temporal variations in  $\alpha_s$  from measurements and Wang (3) from high-resolution simulations. These studies considered Geldart A particles in a narrow geometry. In the present study, the fluctuation characteristics of the solid volume fraction for Geldart B particles in a slightly wider geometry were evaluated from results of Eulerian-Eulerian CFD simulations and from measurements.

## EXPERIMENTS

The solids volume fraction was determined for experiments conducted in a 2D CFB unit at Åbo Akademi University (Guldén, (4)). The height of the riser was 3 m and the width 0.4 m. The distance between the riser walls was 0.015 m which renders the bed pseudo-two-dimensional. The effect of wall friction on the solids is largest at the riser bottom. In the upper dilute regions, flow patterns tend to become three-dimensional. The width 0.015 m is thus a compromise selected to reduce these phenomena. The air distributor consisted of 8 equally spaced air nozzles. Solids exit the riser from the top end and they are separated in a simple separation box from which particles fall through the downcomer into a loop seal consisting of two fluidized 0.1 m wide sections. Experiments were carried out with different particle sizes, solids loads and fluidization velocities. In the present paper, a summary of the experimental findings related to the variation in the solids volume fraction is presented.

In the experiments, a dense vigorously fluctuating bottom region was observed with the highest particle concentration near the side walls. Above the bottom zone, the suspension travelled mainly upwards in a form of clusters and a more dilute suspension between the clusters. At the side walls, the particles fell down either as clusters or as a thin, more continuous wall layer.

Figure 1 illustrates the flow structure in the bottom section (height 0.03-0.34 m above the air distributor) and in a section higher up (height 1.14-1.45 m). A denser wall region with falling clusters can be recognized at both heights. The images show clusters and strands everywhere in the bed. The widths of the narrowest strands observed were approximately 2 mm. At the higher elevation, the solid concentration inside the clusters was significantly lower than in the clusters of the bottom region.

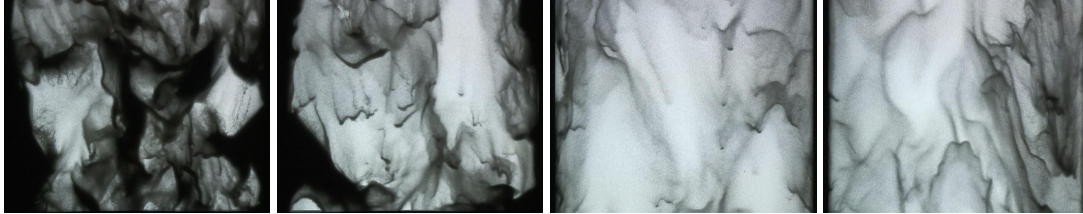


Figure 1. Images from two experiments, from the left: at the bottom for superficial gas velocity  $U_0=2.75$  m/s, at the bottom for  $U_0=3.5$  m/s, at 1.14-1.45 m height for  $U_0=2.75$  m/s, and at 1.14-1.45 m height for  $U_0=3.5$  m/s. Particle diameter is 0.256 mm.

The behaviour of the particles in the CFB unit at these two heights was recorded with a digital video camera that has the image resolution of 720x576 pixels. For each case, a 30 s section of the video was analyzed to estimate the average solids volume fractions and the characteristics of the fluctuations in the chosen locations. The local instantaneous solid volume fraction  $\alpha_s$  was estimated based on a comparison between the local instantaneous grey scale values of the video image with the reference values corresponding to an empty bed and to a packed bed. The same method was used e.g. in Grasa & Abanades (5). Before determining local solids volume fractions, the grey scale values were smoothed with a 3x3 pixel Gaussian filter. The used pixel filter corresponds to 1.7 mm scale in the experimental device.

In Figure 2, the lateral spatial distribution of the average solids volume fraction is plotted at three heights in the bottom bed region and at 1.14-1.45 m height. The average particle size in this case is 0.256 mm, fluidization velocity 2.75 m/s and the solids loading in the riser 120 kg/m<sup>3</sup>. According to Figure 2, a thick wall layer is formed on both side walls at both heights.

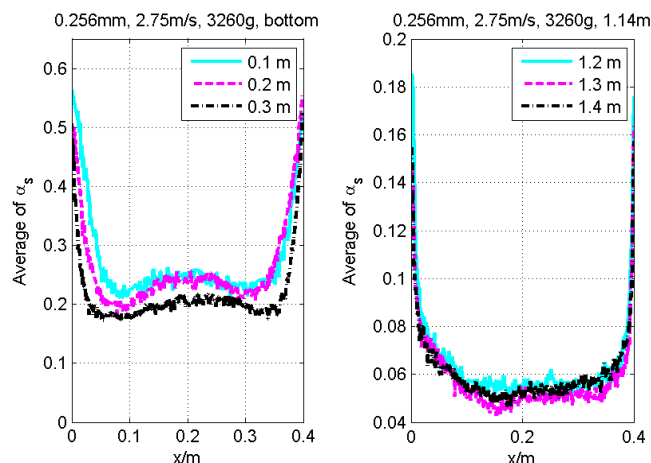


Figure 2. Experimental lateral profiles of the average solids volume fraction at three heights in the bottom bed region (left) and at 1.2-1.4 m height. Particle diameter is 0.256 mm and fluidization velocity 2.75 m/s.

A more detailed analysis of the volume fraction fluctuations can be done by examining the distribution of the instantaneous solids volume fraction. This analysis can be used to identify

different flow regimes and to explain observed behaviour. The probability distributions of the instantaneous solids volume fraction are presented in Figure 3 for two heights. In the dilute area at 1.24 m height, the local solids volume fraction is always in the dilute range, whereas in the bottom zone it varies more and a bimodal distribution is typical. At the walls in the bottom bed, dense suspension regions dominate.

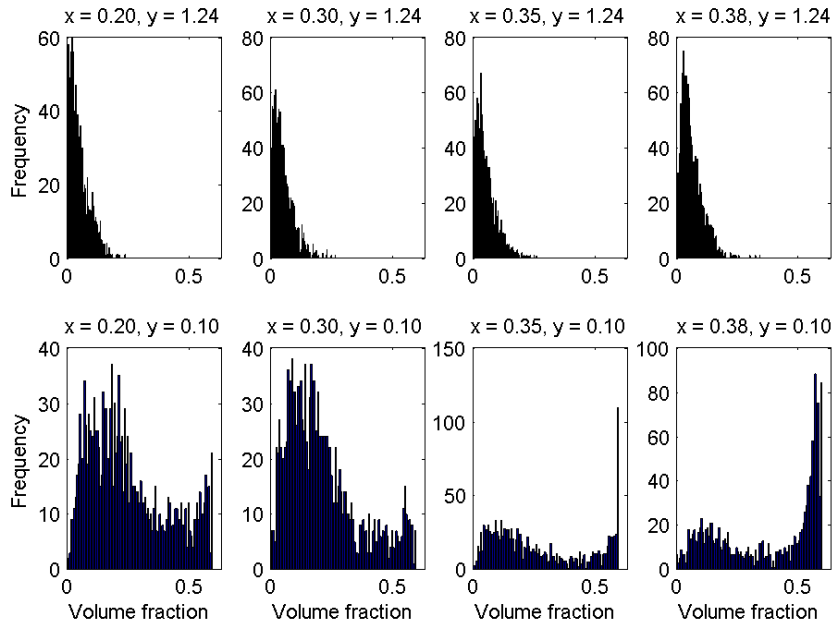


Figure 3. The histograms of the solids volume fraction at 1.24 m height (top) and at 0.1 m height (below). Lateral location varies from  $x=0.20$  m (middle of the riser) to  $x=0.38$  m (0.02 m from the right wall) ( $x$  goes from left to right, cf. Figure 2). Particle diameter is 0.256 mm and fluidization velocity 2.75 m/s.

The standard deviation of the volume fraction

$$\sigma_{\alpha} = \sqrt{(\alpha_s - \overline{\alpha_s})^2} \quad (1)$$

describes the level of time-averaged fluctuation in the solids volume fraction as an easily comparable number. Hence, if the minimum and maximum values of the variable are known, the highest value of the standard deviation it can reach is determined by the mean value. For the solids volume fraction in a granular flow, the theoretical maximum standard deviation is

$$\sigma_{\alpha, \max} = f(\overline{\alpha_s}) = \sqrt{\overline{\alpha_s} (\alpha_{s, \max} - \overline{\alpha_s})}, \quad (2)$$

where the  $\alpha_{s, \max}$  is the packing limit for the solid particles. The theoretical maximum standard deviation tends to zero at the dense and dilute limits and has a maximum of  $\alpha_{s, \max} / 2$  at  $\overline{\alpha_s} = \alpha_{s, \max} / 2$ .

In Figure 4, the standard deviation of the volume fraction, calculated from the same experiment as illustrated in Figure 2, is plotted at the same three heights in the bottom bed region and at 1.14-1.45 m height. In the bottom bed region, the fluctuations in the solids volume fraction are smallest close to the wall while the highest values are observed at the edge of the wall layer. Higher up in the riser the pattern is completely different. The biggest fluctuations are observed on the walls, while in the centre section the fluctuations are relatively small.

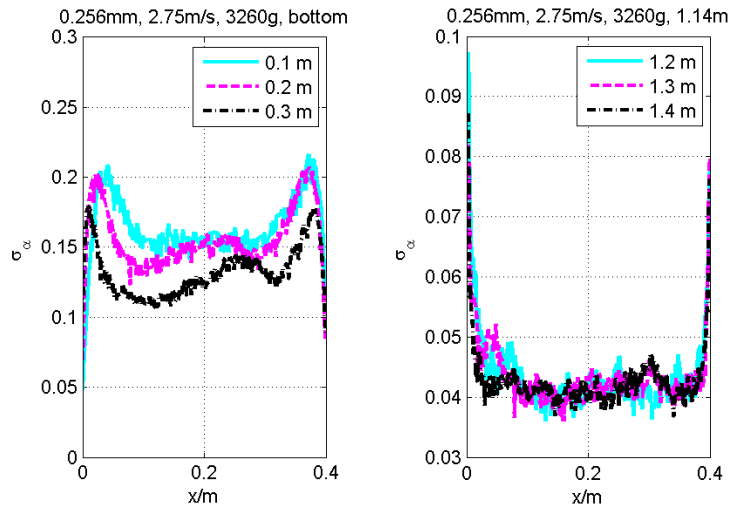


Figure 4. Experimental lateral profiles of standard deviation of the solids volume fraction at three heights in the bottom bed region. Bed mass on the riser side is 1.94 kg, particle diameter 0.256 mm, and fluidization velocity 2.75 m/s.

Wang (3) plotted the standard deviation as a function of the local average solids volume fraction. In the dilute and dense regions, the fluctuations were clearly smaller than in the intermediate suspension density range. The shape of the curves was observed to be close to parabolic which can be expected because of the relationship of the mean and the standard deviation definition, Equation (1). A similar analysis of the experimental data is carried out here. Since the lateral position and the distance to the walls could also play a role in the fluctuation characteristics of the suspension, the wall region data (less than 0.02 m from the walls) were considered separately. Due to the experimental arrangement, solids volume fraction could not be measured in points where the distance to the wall was below 2-4 mm. The effect of the lateral location on the relationship between average  $\sigma_\alpha$  and  $\alpha_s$  is shown in Figure 5 for three cases.

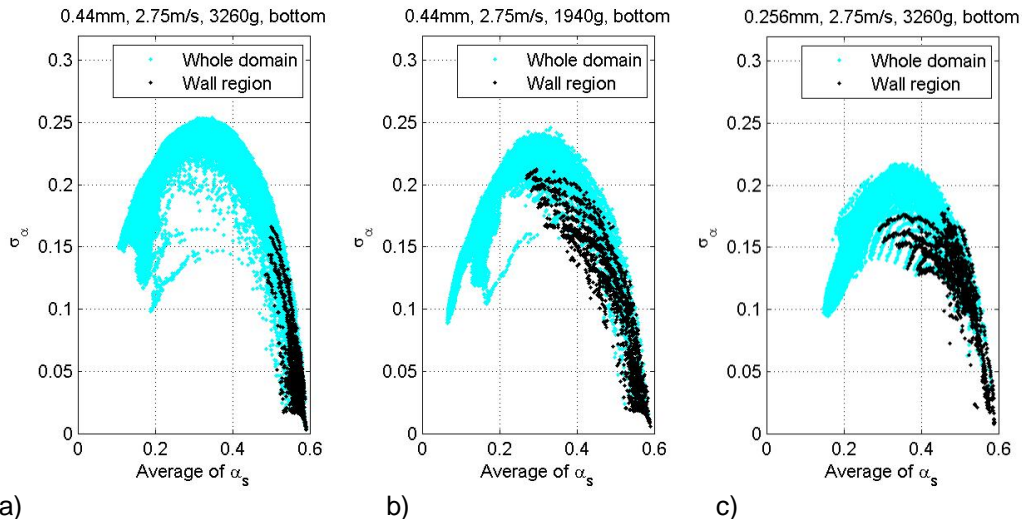


Figure 5. The effect of the lateral location on the relationship between average  $\sigma_\alpha$  and average  $\alpha_s$  in the bottom section in the experiments.  $U_0=2.75$  m/s. Particle diameter: a) and b) 0.44 mm and c) 0.256 mm. Total solids mass in a) and c) 3260 g, and in b) 1940 g.

A high value of the standard deviation indicates extensive clustering and separation into dense and dilute suspension flows. Figure 5 indicates that both the bed mass and the

average particle size affect the clustering of the suspension. A smaller bed mass and a smaller particle size both reduce the maximum value of the standard deviation, indicating that the suspension has become more homogeneous in the experiments. Another reason for the lower measured standard deviations with the smaller particles is the finer cluster structures they produce. These can be partially filtered out by the Gaussian filter used for smoothing the images.

## CFD SIMULATIONS

### Simulation models

The experiments conducted in the 2D CFB were simulated with the models based on the kinetic theory of granular flow available in the Fluent 6.3.26 CFD software (6). In addition, wider fictitious geometries were simulated for comparison. The continuity and momentum equations used in the transient simulations can be summarized for phase  $q$  (gas phase denoted by  $g$  and solid phase by  $s$ ) as follows:

$$\frac{\partial \alpha_q \rho_{qm}}{\partial t} + \frac{\partial \alpha_q \rho_{qm} u_{q,k}}{\partial x_k} = 0 \quad (3)$$

$$\begin{aligned} \frac{\partial \alpha_q \rho_{qm} u_{q,i}}{\partial t} + \frac{\partial \alpha_q \rho_{qm} u_{q,k} u_{q,i}}{\partial x_k} = & -\alpha_q \frac{\partial p}{\partial x_i} + \frac{\partial \alpha_q \tau_{q,ik}}{\partial x_k} + \frac{\partial \alpha_q \tau^M_{q,ik}}{\partial x_k} - \frac{\partial p_q}{\partial x_i} \delta_{qs} \\ & + \alpha_q \rho_{qm} g_i + (-1)^{(\delta_{qs}+1)} K_{gs} (u_{g,i} - u_{s,i}) \end{aligned} \quad (4)$$

where  $t$  is time,  $x$  is spatial coordinate,  $\alpha$  volume fraction,  $\rho$  density,  $u$  velocity,  $p$  gas phase pressure,  $p_s$  solids pressure,  $g$  gravitational acceleration,  $K$  drag coefficient,  $\delta_{qs}$  Kronecker delta,  $\tau$  the laminar stress, and  $\tau^M$  the local scale turbulent stress.

The granular temperature was obtained from a partial differential equation using the Syamlal et al. (6) model for the granular conductivity. The solid phase granular viscosity was calculated from the model by Syamlal et al. (7). The solids bulk viscosity and solids pressure were calculated from the formulas by Lun et al. (8) ( $\alpha_{s,max} = 0.63$ ). The k- $\epsilon$  turbulence model producing the local scale turbulent stress was the version modified for multiphase flows ("dispersed turbulence model", Fluent (6)). At the walls, the partial slip model of Johnson and Jackson (9) was used for the solids with the specular coefficient equal to 0.001 and the free slip boundary condition was used for the gas. For the gas-particle interaction, a combination of the Wen & Yu (10) (at the voidage above 0.8) and Ergun (11) equations was used. The frictional solids stresses were calculated from the model of Schaeffer (12). The first-order discretization for time stepping and the second-order spatial discretization were employed. The time step in the simulation was 0.2 ms. Air inflow velocity at the bottom was described by a function that reproduces the orifice locations.

### Analysis of the fluctuation of solids volume fraction

The results were analysed and plotted in the same way as the experimental data in Figure 5. In Figure 6, results from two simulations with different particle sizes are depicted. In addition to the difference in particle size, the simulations differ in terms of the mesh spacings used in the simulations. For the larger 0.385 mm particles, the mesh spacing was 6.25 mm, whereas in the case of the small 0.256 mm particles, the bottom section (< 0.7 m) of the riser was simulated with a finer mesh with a 3.12 mm spacing. As in the experiments, in dense and very dilute flow regions in the simulations, the fluctuations in the solids volume fraction are small whereas in the intermediate suspension density range fluctuations are large due to the strong clustering tendency of gas-solids suspensions.

The results from the two simulations look similar. The highest values in the standard deviation are located very close to the volume fraction of 0.315, predicted by Equation (2), and consistent with the experiments. In both the simulation cases, fluctuations are reduced close to the walls. Similar reduction was also seen in the experiments, but there the observed wall effect was smaller (Figure 5) since no measurement data could be obtained from the near-wall region (less than 2-4 mm from the side walls). The highest value of  $\sigma_\alpha$  is smaller in the case of the larger particles. This is opposite to what was observed in the experiments where smaller particles produced a more uniform suspension. In the simulations, the difference in the obtained  $\sigma_\alpha$  can also be a result of the differences in the mesh spacings as indicated by the results for the case of a varying mesh spacing in Figure 6. The coarser mesh used in the simulation with larger particles does not resolve the finest clusters and this could produce a more uniform suspension in the simulation. This effect of the mesh on  $\sigma_\alpha$  was confirmed by conducting simulations in coarser meshes. In the future, simulations in finer meshes should be conducted to evaluate effects of the particle size.

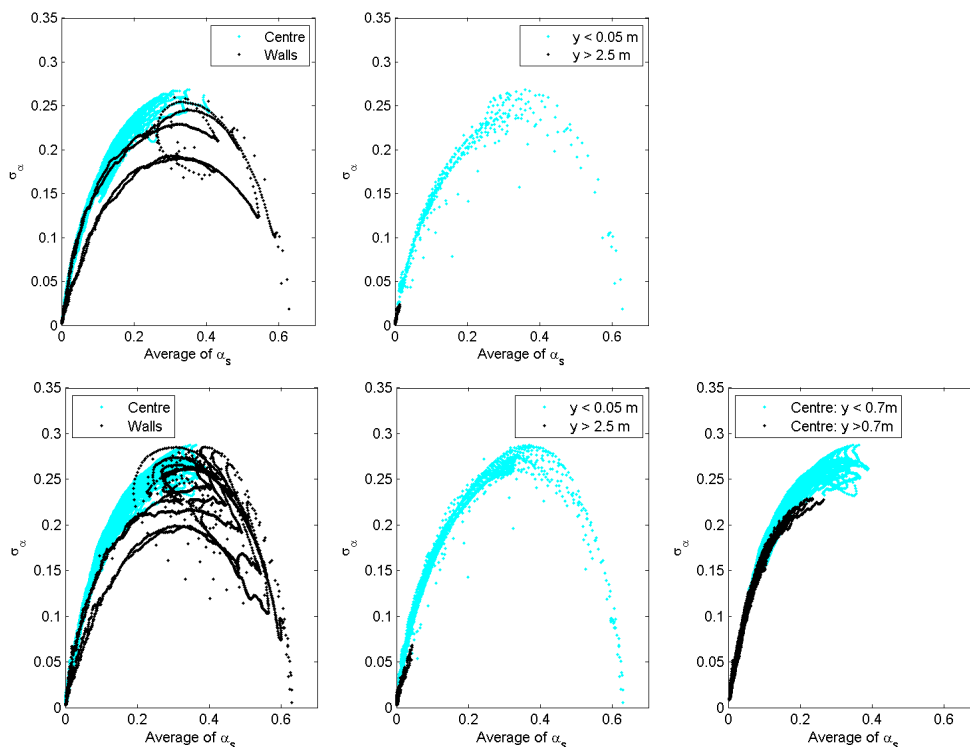


Figure 6. Average fluctuation in the solids volume fraction as a function of the average solids volume fraction plotted for different regions in simulations of 2D CFB experiments with fluidization velocity 3.15 m/s and particle size 0.385 mm (top) and fluidization velocity 2.75 m/s and particle size 0.256 mm (below). 'Walls' refers to a 0.015 m wide layer at the side walls. 'Centre' refers to the whole domain without the 0.05 m high bottom section, the 0.015 m wide wall sections, and a 0.05 m high section at the top exit.

The same analysis of the temporal distribution of the solids volume fraction carried out with the experimental results (Figure 3) was also repeated with the simulation data. Figures 7 and 8 show the probability distribution of the solids volume fraction and its logarithm in the core region and close to the walls for a few monitoring points. The points represent different suspension regimes.

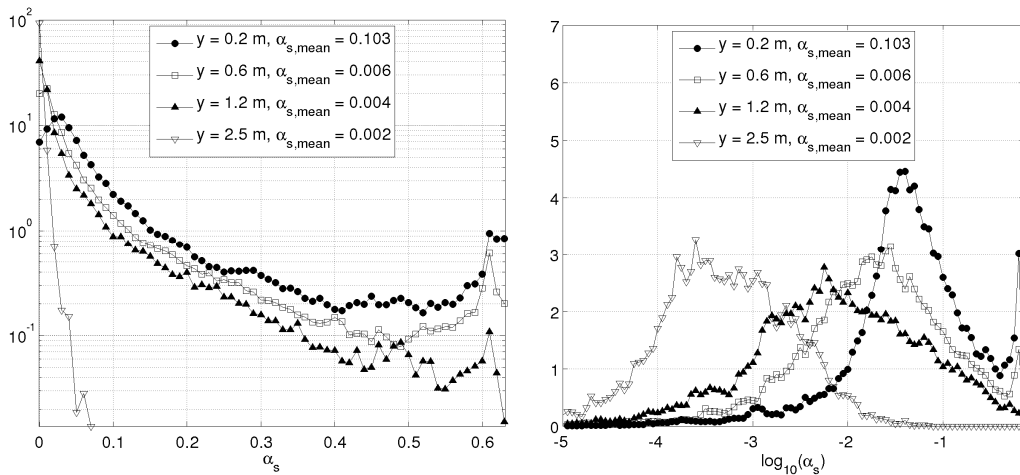


Figure 7. Probability distributions of solids volume fraction (left) and logarithm of the solids volume fraction (right) in the riser core region at different heights in a CFD simulation. Fluidization velocity 3.15 m/s and particle size 0.385 mm

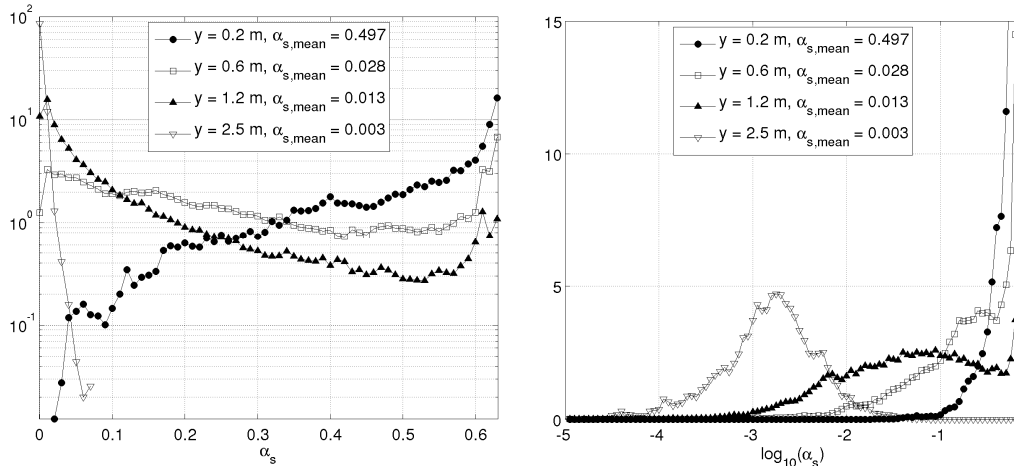


Figure 8. Probability distributions solids volume fraction (left) and logarithm of the solids volume fraction (right) close to the riser side wall (at  $x=0$ ) at different heights in a CFD simulation. Fluidization velocity 3.15 m/s and particle size 0.385 mm.

Examining probability distributions for a number of points, three distinct types of probability distributions can be defined and used to identify three different suspension density regimes. Firstly, for lower time-averaged volume fractions than 0.01, no volume fraction values close to the packing limit occur and the mode of the volume fraction distributions is very close to zero. In this case, the probability distributions of  $\log(\alpha_s)$  resemble the normal distribution. In this “dilute” suspension regime, the volume fraction fluctuations are not affected by the packing limit.

Secondly, at average solids volume fractions above 0.03 and below 0.3, there are distributions that have distinct modes at very low volume fractions and right at the packing limit. The distributions of the  $\log(\alpha_s)$  consist of a dilute sub-distribution resembling the normal distribution and a sharp peak at the packing limit (Figures 7 and 8). As the average solids volume fraction increases, the dilute mode moves toward the packing limit mode and the packing limit peak grows until the modes merge. In this “bimodal” suspension regime, the formation of densely packed clusters significantly affects the flow behaviour. The standard deviation of the solids volume fraction increases as the mean value increases and reaches its peak values just before the two modes merge.



Thirdly, in the “dense” suspension regime the average solids volume fraction is above 0.35 and there is only one mode in the volume fraction probability distribution: the peak at the packing limit. As the mean solids volume fraction increases, the distribution narrows towards the packing limit reducing the volume fraction fluctuations.

## CONCLUSIONS

In the paper, the variation of the solids volume fraction in measurements and simulations of a 2D CFB was analysed. Both the measured and simulated results showed very similar characteristics. In dense and very dilute flow regions, the fluctuations in the solids volume fraction are small whereas in the intermediate suspension density range fluctuations are large due to the strong clustering tendency in gas-solids suspensions. The probability distribution of the temporal solids volume fraction is characterized by different shapes for the dilute, bimodal and dense suspensions.

## ACKNOWLEDGMENT

The authors gratefully acknowledge the financial support of Tekes, VTT Technical Research Centre of Finland, Fortum Oyj, Foster Wheeler Energia Oy, Neste Oil Oyj and Metso Power Oy.

## NOTATION

$g$	gravitational acceleration [ $m/s^2$ ]	<i>Subscripts</i>	
$K_{gs}$	momentum exchange coefficient [ $kg/s^2m^3$ ]	$f$	gas phase
$p$	pressure [ $N/m^2$ ]	$q$	phase index
$t$	time [s]	$s$	solid phase
$u, \mathbf{u}$	velocity [ $m/s$ ]	$x, y, z$	rectangular coordinates
$U_0$	superficial velocity [ $m/s$ ]	<i>Other symbols and operators</i>	
$\alpha$	volume fraction [-]	$\nabla$	gradient operator
$\delta$	Kronecker delta	$\bar{x}$	time average of $x$
$\rho$	material density [ $kg/m^3$ ]		
$\sigma$	standard deviation		
$\tau$	stress tensor [ $N/m^2$ ]		

## REFERENCES

- Bai, D., Issangya, A.S., Grace, J.R., Ind. Eng. Chem. Res. 38 (1999) 803-811.
- Issangya, A.S., Grace, J.R., Bai, D., Zhu, J., Powder Technology 111 (2000) 104-113.
- Wang, J., Chemical Engineering Science, 63 (2008) 3341-3347.
- Guldén, M. Pilotmodell av en cirkulerande fluidiserad bädd, Masters thesis (in Swedish), Åbo Akademi Univ., Heat Engineering Lab., Turku, Finland, 2008.
- Grasa G. and Abanades J.C., Powder Technology, Vol. 114 (2001) 125-128.
- Fluent Inc., Fluent 6.3 Users manual (2006).
- Syamlal, M., Rogers, W., and O'Brien T. J. *MFIX Documentation: Volume 1, Theory Guide*. National Technical Information Service, Springfield, VA, DOE/METC-9411004, NTIS/DE9400087 (1993). (Referenced by Fluent (6)).
- Lun, C. K. K., Savage, S. B., Jeffrey, D. J., Chepur, N. *J. Fluid Mech.*, Vol. 140 (1984) 223-256. (Referenced by Fluent (6)).
- Johnson, P.C., Jackson, R. *J. Fluid Mech.*, Vol. 176 (1987) 67-93.
- Wen, C.Y., Yu, Y.H., Chemical Engineering Progress Symposium Series, Vol. 66 (1966) No. 62, pp. 100-111.
- Ergun, S., Chemical Engineering Progress, 48 (1952) 89-94.
- Schaeffer, D. G. *J. Diff. Eq.*, Vol. 66 (1987) 19-50. (Referenced by Fluent (6)).